SCIENCE CHINA
Chemistry

•ARTICLES•

https://doi.org/10.1007/s11426-025-2736-7

Persistent and ultrastable chemiluminescence "super enriching" on single microbead for sensing attomolar biomarkers

Chao Lei, Wenjiao Fan, Wei Ren, Xinrui Duan* & Chenghui Liu*

Key Laboratory of Applied Surface and Colloid Chemistry, Ministry of Education, Key Laboratory of Analytical Chemistry for Life Science of Shaanxi Province, School of Chemistry and Chemical Engineering, Shaanxi Normal University, Xi'an 710019, China

Received February 10, 2025; accepted April 27, 2025; published online July 24, 2025

We propose a novel single microbead "chemiluminescence (CL) super enriching and imaging" strategy that efficiently concentrates highly intense, long-lasting, and ultrastable CL shining on only a single microbead (SMB), allowing for the ultrasensitive quantification of various biomarkers at the attomolar level. Aided by a phenothiazine derivative enhancer, the traditional flash-type CL of horseradish peroxidase (HRP)-H_2O_2-luminol can be efficiently converted into a significantly enhanced (10^3-fold), persistent, and ultrastable CL emission (E-CL) that can be exactly confined and accurately imaged on the microbead interface. Then, by employing only one minuscule-sized SMB as the sole reaction and signaling unit, the target as well as the aroused E-CL signal concentrated on the SMB can further achieve ~10^4 "super-enriching" efficiency. Therefore, by "super enriching" target-responsive E-CL signal on an SMB, the SMB E-CL imaging strategy provides a powerful tool for the attomolar-level detection of various biomarkers including proteins, microRNAs, and virus DNA.

single microbead analysis, long-lasting chemiluminescence, immunoassay, microRNA, super enriching

Citation: Lei C, Fan W, Ren W, Duan X, Liu C. Persistent and ultrastable chemiluminescence "super enriching" on single microbead for sensing attomolar biomarkers. *Sci China Chem*, 2025, 68, https://doi.org/10.1007/s11426-025-2736-7

1 Introduction

Accurate quantification of extremely low levels of key biomarkers in body fluids, such as disease-associated nucleic acids and proteins, is becoming increasingly important for early disease screening and postoperative efficacy monitoring [1–6]. Compared with traditional bulk measurement-based homogeneous bioassays, microbead-based bioassays have shown unique advantages because the beads can capture and separate the target molecules from complex biological samples to effectively avoid interference [7–9]. Meanwhile, the minuscule-sized microbeads bearing the target-enriched signaling molecules can be interrogated as individual signal-readout units with improved sensitivity, through flow cytometry or imaging-based microbead counting [10–14]. Nevertheless, such microbead-based bioassays mainly rely on fluorescence signal reading or counting, in which the scattering background of the excitation light, self-quenching, and particularly, potential photobleaching can hardly be avoided [15–17]. Additionally, they are generally conducted with a large number of beads in one reaction, making the diluted signal arising from ultralow-level target molecules on each bead barely detectable.

Superior to photoexcited fluorescence, chemiluminescence (CL) can get rid of photobleaching and scattering background since no external excitation light is required, intrinsically permitting a much higher signal-to-background ratio and sensitivity [18–23]. However, most biocompatible CL systems (such as the luminol-H_2O_2 system) display flash-type emissions that last for minutes or even seconds with a fast signal decay, making it difficult to apply to imaging or counting-based quantification since the unavoidable fluc-

*Corresponding authors (email: duanxr@snnu.edu.cn; liuch@snnu.edu.cn)

tuation at the initial/terminal stages will severely affect the detection accuracy [24–26]. Despite several strategies have been proposed to enhance the traditional luminol-H_2O_2 CL emission, such as chemical co-reactant optimization [27,28], engineered nanomaterials [29–33], using of peroxidase-mimicking nanozymes [34] and catalytic ion regulation [35], these advancements primarily focus on improving the total CL intensity through accelerated reaction kinetics. Recently, a long-lasting CL mechanism has been proposed by physically controlling reactant diffusion through a porous structure [25,36,37]. However, this method still faces challenges in the standardization of porous CL material preparation, precise control of pore structure, and signal stability. Alternatively, the enhancer-assisted, enzyme-based long-lasting CL systems that rely on continuous enzyme catalytic action provide a more suitable pathway for biomarker analysis [38,39]. Nevertheless, due to challenges such as biocompatibility issues, insufficient signal stability, environmental adaptability, and limitations of CL enhancers, how to realize long-term stable and sustained CL emission remains a critical issue, particularly for imaging/counting-based bioapplications.

Moreover, unlike fluorescent labels that can be directly anchored on the microbead to yield detectable signals, the signal output of the CL system relies on multiple cascaded chemical reactions. Though some microbead-based CL strategies have been reported [34,40–43], these studies solely employed numerous microbeads as carriers for CL reactants/catalysts accompanied by bulk CL signal measurements. Technically, it is challenging but of great significance to precisely image the target-responsive CL signal confined on the surface of microbeads with single-particle resolution.

In this work, we have developed a new generation of single microbead (SMB) "super enriching" enhanced-CL (E-CL) imaging system that enables highly intense, long-lasting, and ultrastable CL signal confined around the interface of an SMB, allowing for the ultrasensitive detection of a broad range of biomarkers down to the attomolar level. Specifically, this innovative method features the following advantages: (1) Just following simple standard workflows of immunoreaction or nucleic acid hybridization, the target as well as the target-responsive HRP will be concentrated on the surface of only one SMB, achieving approximately 10^4 "super-enriching" efficiency from a 2 μL solution. (2) With the help of a phenothiazine derivative enhancer, the conventional flash type CL of the HRP-H_2O_2-luminol system is converted to remarkably enhanced, persistent emission that can last for hours. More importantly, the target-introduced HRP on the SMB's surface can continuously catalyze the interfacial E-CL reaction and maintain strong, persistent, and ultrastable CL emission around the microbead, which allows for much longer exposure time for signal acquisition and handy operation for imaging, ensuring high accuracy for detecting ultralow concentrations of target molecules. (3) The proposed method can be further integrated with other signal amplification methods (*e.g.*, tyramine signal amplification (TSA)) to improve the sensitivity and broaden the dynamic range. As a result, this work achieves attomolar level sensitivity in detecting both protein and nucleic acid biomarkers. To the best of our knowledge, this is the first report to realize ultrastable interfacial CL imaging coupled with the single microbead-based "super enriching" strategy, which opens a new route to the ultrasensitive detection of extremely low-abundance critical biomarkers.

2 Experimental

2.1 Materials and reagents

All nucleic acid oligonucleotides (Table S1, Supporting Information online) were synthesized by Sangon Biotech (Shanghai, China). Prostate cancer antigen (PSA), alpha-fetoprotein (AFP), cardiac troponin I (cTnI), carcinoembryonic antigen (CEA), Goat anti-Mouse IgG (IgG) and their specific antibody pairs used in this study were obtained from Linc-Bio Science (Shanghai, China). Streptavidin-modified polyHRP (STV-polyHRP) was purchased from Thermo Fisher Scientific (WA, USA). The *N*-hydroxysuccinimide Mag Sepharose microbeads (NHS-MBs) were obtained from GE Healthcare (Uppsala, Sweden). Biotin-HRP and HRP were supplied by Sangon Biotech (Shanghai, China). Luminol was purchased from Aladdin (Shanghai, China). Hydrogen peroxide (H_2O_2, 30%) was purchased from KeyGEN BioTECH (Jiangsu, China). TSA Biotin Reagent Pack (containing biotin-tyramide and 1 × TSA buffer) was purchased from Beijing Biodragon Immunotechnologies Co., Ltd. The E-CL solution used in this study, which contains a phenothiazine derivative enhancer ($C_{15}H_{14}O_3NS_2Na$) to enhance CL performance, is self-developed and now commercially available from Yingtaisheng Biotech (Xi'an, China).

2.2 Preparation of capture antibody (or DNA probe)-conjugated SMB (SMB-mAb1 or SMB-cDp)

Single microbeads of the appropriate size (80 ± 5 μm) are manipulated using a Narishige micro-operating system installed on an Olympus IX 53 inverted microscope. 20 uniform NHS-MBs were selected and placed in a tube, followed by adding 100 μL of 1 mM cold HCl to activate their NHS surface. After purification, 0.1 μg mAb1 (or 1 pmol NH_2-modified capture DNA probe) was added into the tube, and incubated with the microbeads for 1 h with gentle shaking. After that, 100 mM Tris was used to effectively block the excessive active sites on the surface of the microbeads. Afterward, 100 μL 1 × PBST (0.05% Tween) was

used to wash and purify the labeled microbeads. Finally, uniformly modified single microbeads were transferred one by one to each reaction tube containing 1 × PBST-BSA (0.05% Tween, 1% BSA) before standard assays.

2.3 Standard protocols for the SMB-based immunoassay

For the amplification-free immunoassay, the SMB-mAb1 was reacted with a 2 μL PBST-1% BSA (PBS with 0.05% Tween-20 and 1% BSA) solution containing serially diluted target antigen and biotinylated detective antibody (100 pg) for 2 h at room temperature with violent shaking. Then the reacted SMBs were washed three times using PBST-1% BSA solution, with gentle mixing to ensure complete removal of unbound reagents. After purification, the SMB was incubated with a 2 μL solution containing STV-polyHRP (500 pg) for 30 min at room temperature with vigorous shaking to conduct the HRP enzyme labeling reaction. Finally, the SMB was purified and resuspended in 2 μL PBST-5% BSA for interfacial CL imaging.

In the TSA-mediated immunoassay, 0.1 × commercially obtained TSA buffer (containing H_2O_2) was used for biotin-tyramide dilution and TSA amplification. After the HRP labeling reaction mentioned above, the single microbead was incubated successively with 2 μL biotin-tyramide (500 pg) solution and STV-polyHRP (500 pg) solution at room temperature with vigorous vibration for 30 min, respectively. Finally, the single microbeads were purified and resuspended in 2 μL PBST-5% BSA for interfacial CL imaging measurement.

For real sample analysis, the PSA levels in the serum samples provided by two volunteers from our lab were independently tested by the SMB CL imaging strategy and a routine medical diagnostic kit (results tested by the Hospital of Shaanxi Normal University). This study was approved by the Ethics Committee of Shaanxi Normal University, and informed consent was obtained from the participants.

2.4 Standard protocols for nucleic acid detection

For nucleic acid detection, the SMB-cDp was reacted with 2 μL solution containing serially diluted target microRNA or DNA and the biotinylated detective probe (1 nM) for 2 h at room temperature with shaking. The subsequent steps were identical to the protein detection procedures.

2.5 Single microbead interfacial CL imaging

After the immunoreaction or nucleic acid binding reaction stated above, a single microbead labeled with target dose-responsive poly-HRP was mixed with the E-CL solution (100 mM Tris-HCl (pH 9.0) containing luminol, H_2O_2 and the enhancer), followed by placing it on a piece of the glass slide. Bright-field imaging was carried out for the SMB positioning. Then all subsequent measurements of the single microbead were performed in a dark box. An EMCCD camera (Photometrics) controlled by the Micro-Manager 1.4 plugin in ImageJ was used to record the CL signals at the single microbead location (referring to the bright field image) for CL imaging (Bright field imaging parameters: Exposure at 4 ms, Binning at 1, Gain at 1, and Gain EM at 1. CL imaging parameters: Binning at 1, Gain at 3, and Gain EM at 150). Finally, analysis of the single microbead CL images was performed using ImageJ software.

For comparison, conventional CL signals generated in homogeneous solutions were recorded using an RFL-T ultraweak chemiluminescence/bioluminescence detector (Xi'an Remax Analytical Instruments Co., LTD.).

3 Results and discussion

3.1 Characteristics of persistent and ultrastable E-CL in solution and SMB interface

The catalytic mode of the typical luminol-H_2O_2-HRP CL system can be graphically described as a "molecular factory" (left panel of Figure 1a). H_2O_2 provides HRP energy, thus driving HRP gear rotation and promoting the conversion of luminol from the ground state to its excited state, and finally generating CL signal (Eqs. (1) to (6) in Figure S1, Supporting Information online). Due to the intrinsic low catalytic efficiency of HRP on luminol and irreversible consumption of HRP activity, weak flash-type CL signals are generated, which is unfavorable for improving the accuracy and sensitivity of bioassays or achieving high-quality imaging analysis. Fortunately, the incorporation of a phenothiazine derivative enhancer, which exhibits excellent redox reversibility and free radical stabilization capacity due to its sulphury atom and conjugated aromatic structure, can significantly amplify the HRP turnover rate and the equivalent concentration of the pivotal luminol anion radical, the origin of CL [44,45]. This process is crucial because the enhancer acts as a superior substrate for HRP, facilitating the generation of a high-energy intermediate. This intermediate can swiftly transfer energy to luminol, akin to a gear mechanism where the intervention of the "enhancer gear" (the right panel of Figure 1a) dramatically accelerates the HRP's conveyance of luminol to its excited state, resulting in long-lasting and greatly enhanced CL (E-CL, see detailed Eqs. (7)–(9) in Figure S1). We have experimentally evaluated the properties of the E-CL system in the homogeneous solution. As shown in the schematic diagram of Figure 1b and Figure S2, compared with the conventional luminol-H_2O_2-HRP system, the enhancer-assisted E-CL system can provide a much more intense, prolonged, and stable light output in the homogeneous system. Even with 3 orders of magnitude lower

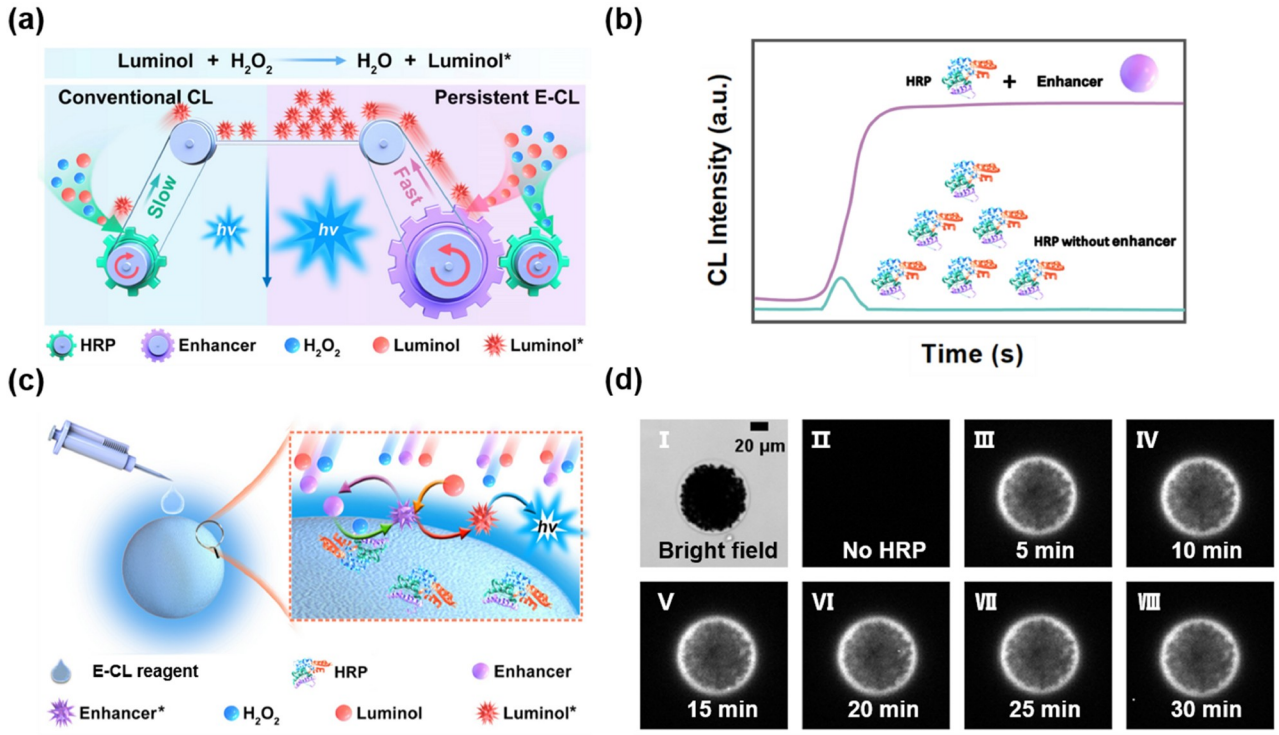

Figure 1 (Color online) Schematic illustration of the new E-CL system. (a) Schematic diagram of the luminol-H_2O_2 CL system catalyzed by HRP alone (blue background) and HRP-enhancer (purple background), respectively. (b) Schematic diagram of the CL intensity over time catalyzed by HRP in the presence and absence of enhancers. The "flash-type CL" curve illustrates a scenario with abundant HRP but no enhancer, represented by a transient emission. In contrast, the "stable and long-lasting CL" curve, achieved with a much lower HRP content and the addition of an enhancer, exhibits a stronger, more durable and consistent emission. (c) Schematic diagram of the enhancer-assisted CL reaction (E-CL) on a single microbead's interface (Enhancer*: enhancer radical. Luminol*: Luminol radical). (d) The bright field image (I) and CL images of a single microbead without (II, 5 min incubation time) biotin-HRP immobilized on the surface. The CL images (III–VIII) were acquired from the same SMB with 100 pg biotin-HRP immobilized on the surface at different time points during the E-CL reaction process.

HRP content, much higher signal intensity can still be achieved, and the enhancement in integrated intensity will certainly be more significant, resulting in far more than 10^3-fold signal enhancement.

Since HRP is the catalytic driver of the CL emission, next, we challenged to "super-confine" the E-CL around the SMB surface by rationally enriching HRP on the microbead, while other E-CL reagents remained in the aqueous solution phase, as illustrated in Figure 1c. The redox reversibility of the phenothiazine derivative enhancer facilitates the catalytic cyclic regeneration of HRP at the microbead interface, thereby enabling a self-sustaining mechanism for the CL reaction. The results of Figure 1d and Figure S3 demonstrate that after adding the E-CL reagents, HRP enzymes immobilized on the surface of the SMB will continuously catalyze the cascade E-CL reaction to generate persistent CL at the microbead-liquid interface. Notably, the SMB interfacial CL signal remained remarkably consistent for up to half an hour without obvious decay. This is a significant advancement over traditional flash-type CL systems that are often limited by the quite short luminescence duration. The sustained and stable E-CL signal is extremely suitable for SMB CL imaging toward ultrasensitive biosensing because the CL data collection will not be affected by fluctuations in photography and operation times, and the stability of the signal allows for prolonged integration with easy operation, ensuring enhanced sensitivity and high accuracy. Figure 1c illustrates the mechanism of the SMB interfacial long-lasting CL. While HRP, the central catalytic driver of the CL reaction, is enriched on the SMB surface, the other excessive E-CL reagents in the aqueous phase will continuously diffuse to the SMB interface to supply "fuel" for the HRP. This ensures a consistent, stable, and intense CL signal, the intensity of which is directly correlated with the amount of HRP loaded on the SMB surface. To the best of our knowledge, this is the first time that stable CL imaging at the catalytic interface of an SMB has been achieved, which may open a new way for fabricating ultrasensitive bioassays by "super CL enriching" on an SMB.

3.2 The SMB E-CL imaging-based amplification-free immunoassay

To demonstrate the advantages and potential of SMB-based

"super CL enriching" in ultrasensitive biosensing, we first assessed its performance in immunoassay. As schematically displayed in Figure 2a, first, capture antibody-conjugated SMB can effectively capture the target antigen and further bind with biotinylated detective antibody to form a sandwich immune complex. Subsequently, streptavidin-modified polyHRP (STV-polyHRP) molecules will be captured by the biotinylated detective antibody, introducing HRP to the SMB's surface. Finally, after adding the E-CL solution, the anchored STV-polyHRP molecules catalyze the surrounding CL substrate to produce a "super-enriched and confined" CL signal on the liquid-microbead interface. Since the STV-polyHRP molecules anchored on the surface of the single microbeads are in positive correlation to the dosage of the target antigen, by monitoring the CL intensity via SMB imaging, the quantitative detection of the target antigen can be achieved.

As a proof-of-concept demonstration, prostate cancer antigen (PSA) is chosen as the model target. Under the optimized conditions (Figure S4), the CL images (Figure 2b) show that the brightness around the SMB gets enhanced gradually with the increase of PSA concentration, and the CL signal of the SMB treated with as low as 100 fg mL^{-1} PSA can be clearly distinguished from the blank control. Furthermore, the CL signal of the SMB exhibits a good linear correlation with the PSA concentration in the range of

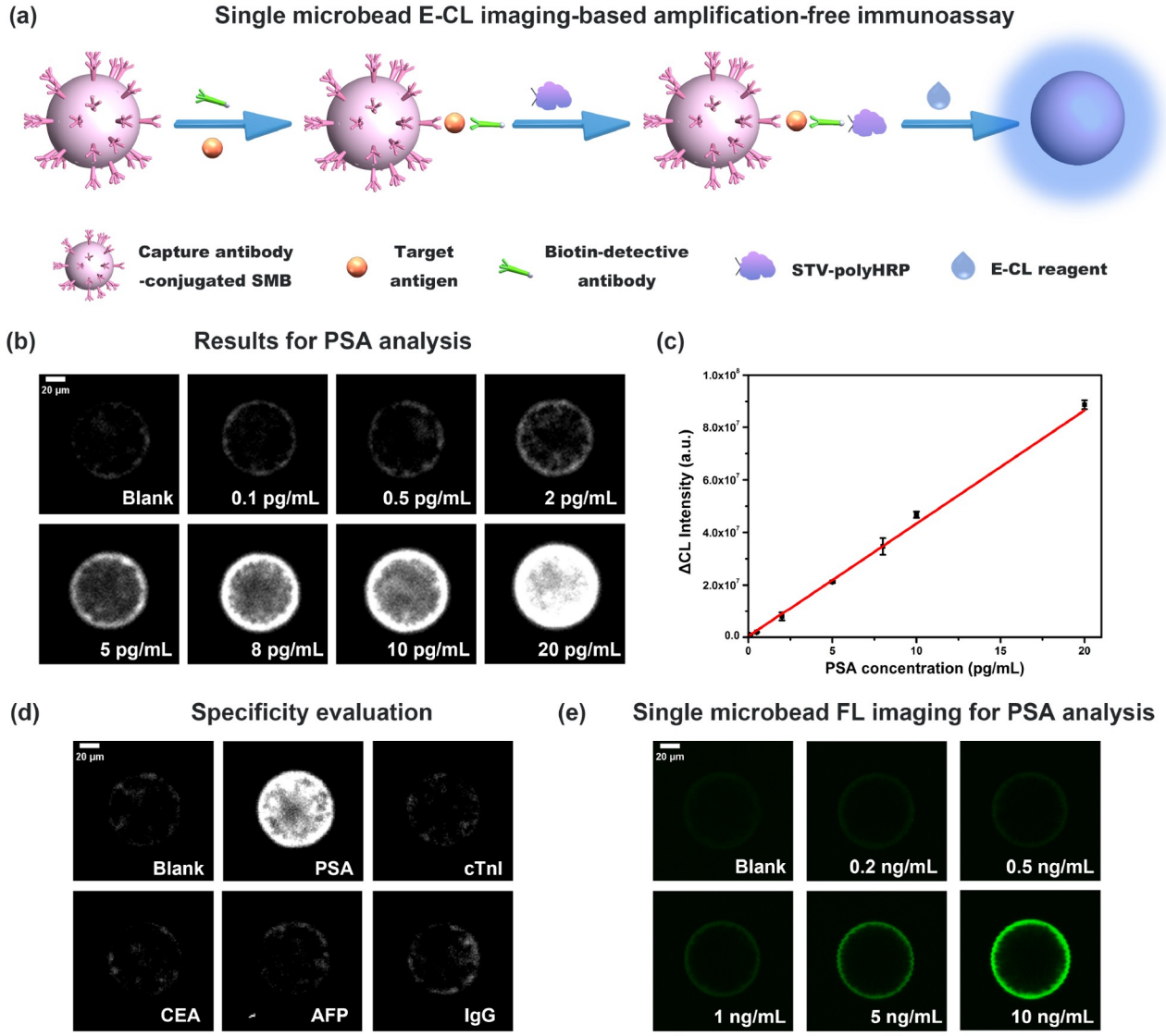

Figure 2 (Color online) (a) Schematic illustration of the proposed single microbead E-CL imaging strategy for amplification-free immunoassay. (b) E-CL imaging results for PSA analysis. (c) The relationship between the ΔCL intensity of the single microbeads and the PSA concentration. ΔCL is the target antigen-produced interfacial CL intensity subtracted by the signal of the blank control. Error bars represent the standard deviation of three independent experiments. (d) Specificity evaluation of the single microbead E-CL imaging system for PSA analysis. E-CL images of the system were acquired in the presence of 10 pg mL^{-1} of different proteins with the PSA-specific antibodies. (e) Single microbead fluorescence (FL) imaging for PSA detection.

100 fg mL^{-1} to 20 pg mL^{-1} (Figure 2c). The linear regression equation is $\Delta CL = 4.29 \times 10^6 C_{PSA} + 3.82 \times 10^5$ (R^2 of 0.994), and the limit of detection (LOD) is calculated to be 25 fg mL^{-1} (3σ). The same standard protocol also shows excellent performance in alpha-fetoprotein (AFP) detection (Figure S5). This proves that by employing the corresponding target-specific antibody pairs, the SMB E-CL imaging strategy can detect different types of antigens just through a simple standard sandwich-type immunoreaction. Furthermore, the specificity of the proposed strategy is investigated by challenging the PSA-specific system with other potential interfering proteins. As shown in Figure 2d and Figure S6, only PSA can trigger a significant CL signal around the SMB, while the responses of other proteins are negligible (similar to the blank control), which clearly indicates the high specificity of the proposed strategy.

The practical application potential of the proposed strategy in real sample analysis is interrogated by detecting the PSA levels in serum samples from two healthy volunteers. The PSA concentrations of the two serum samples are provided by the Hospital of Shaanxi Normal University through a routine medical diagnostic kit, which is determined to be 0.62 ng mL^{-1} (volunteer 1), and 1.10 ng mL^{-1} (volunteer 2) respectively. At the same time, by using our SMB CL imaging strategy, the PSA concentrations of the 2 serum samples are determined to be 0.63 ± 0.08 ng mL^{-1} (volunteer 1), and 0.95 ± 0.02 ng mL^{-1} (volunteer 2), respectively. The results support the reliability of the proposed strategy in the analysis of complex biofluid samples.

3.3 Comparison of SMB E-CL imaging strategy with fluorescence signal readout and multi-microbead sensing system

To further demonstrate the advantages of the proposed SMB CL imaging biosensing strategy, we performed single microbead fluorescence (FL) imaging toward PSA assay for comparison. We conducted the PSA immunoassay by using STV-functionalized CdSe@ZnS quantum dots with strong emission centered at 605 nm as signal reporters. As shown in Figure 2e, the FL signal on an SMB induced by 0.2–0.5 ng mL^{-1} PSA can be just discriminated from the blank control. According to these results, the SMB CL imaging possesses more than 10^3 times higher sensitivity compared with FL detection. What's more, to better illustrate the powerful "super CL enriching" effect by use of an SMB, we also performed multi-microbeads comparison experiments where about 100 microbeads are involved for each reaction. As shown in Figure S7, when the concentration of PSA is lower than 50 pg mL^{-1}, the CL brightness of the multiple microbeads treated with PSA is hardly distinguished from the blank control, indicating a significantly reduced sensitivity compared to the SMB-based method [46,47]. This limitation can be attributed to the distribution of signaling molecules and cumulative background noise across multiple microbeads, which renders ultralow levels of target molecules on each bead barely detectable. Considering the above experimental results, we can attribute the excellent analytical performance of the proposed strategy to the super-enriching capability of the SMB and the powerful, long-lasting, stable, and intense E-CL system.

3.4 TSA-mediated SMB E-CL imaging-based immunoassay

The TSA-mediated amplification technique is introduced to further improve the sensing performance of the SMB CL imaging immunoassay [48,49]. In the presence of H_2O_2, polyHRP will rapidly catalyze the *in-situ* deposition of tyramine on the protein residues adjacent to the polyHRP catalytic site [47,50]. As shown in Figure 3a, polyHRP-activated tyramine-biotin deposition will introduce more target-mediated polyHRP binding events to the surface of an SMB, significantly enlarging the contrast between the target-containing samples and the background, allowing for the detection of extremely low levels of target protein. According to the E-CL imaging results shown in Figure 3b, the CL signal aroused by as low as 2 fg mL^{-1} PSA, which is equivalent to ~70 PSA molecules in a 2 μL system, can be

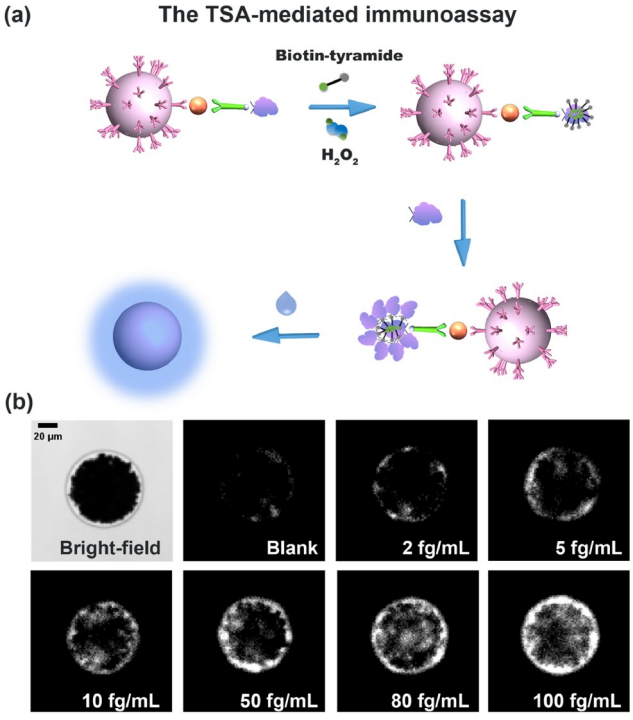

Figure 3 (Color online) (a) Schematic illustration of the proposed SMB E-CL imaging strategy integrated with TSA-mediated amplification for immunoassay. (b) CL images of the single microbeads treated with series concentrations of PSA under the assistance of TSA-mediated amplification.

clearly distinguished from the blank control. As shown in Figure S8, a good linear relationship between the interfacial ΔCL intensity of the SMB and PSA concentration is obtained in the range of 2–100 fg mL^{-1}. The LOD of PSA antigens based on TSA-mediated amplification was defined as ~0.7 fg mL^{-1} (~21 aM). TSA contributes to ~50-fold higher sensitivity, making this method one of the most sensitive immunoassays based on optical signal readout (Table S2). Particularly, it is recognized that the digital immunoassays, represented by the elegant Simoa platform and other single-molecule imaging techniques, are the most sensitive ways for protein analysis even at the single-molecule level. The LODs of PSA (or other proteins) by Simoa or other digital ELISA methods typically fall within the range of 50 aM–10 fM [16,50–54]. Thus, the sensitivity of the SMB CL imaging strategy is superior to or at least comparable to those obtained by the most powerful digital ELISA techniques or other most sensitive optical methods.

3.5 The SMB E-CL imaging-based analysis of nucleic acid

In addition to ultrasensitive protein analysis, we further attempt to apply the SMB CL imaging strategy to microRNA analysis by selecting let-7a as a model target through a simple sandwich-type hybridization reaction (top panel of Figure 4a). As Figure 4a and Figure S9 display, the increasing let-7a concentration leads to gradually increased brightness of the SMB, and as low as 10 fM let-7a can be easily distinguished from the blank control. Notably, the TSA-assisted strategy is also feasible for let-7a analysis. According to the SMB E-CL imaging results shown in Figure 4b, the CL signal aroused by as low as 200 aM let-7a, which is equivalent to ~240 let-7a molecules in a 2 μL system, can be clearly distinguished from the blank control. Therefore, the integration with TSA endows the SMB CL imaging approach with attomolar level sensitivity for microRNA analysis. In addition, the above strategies for

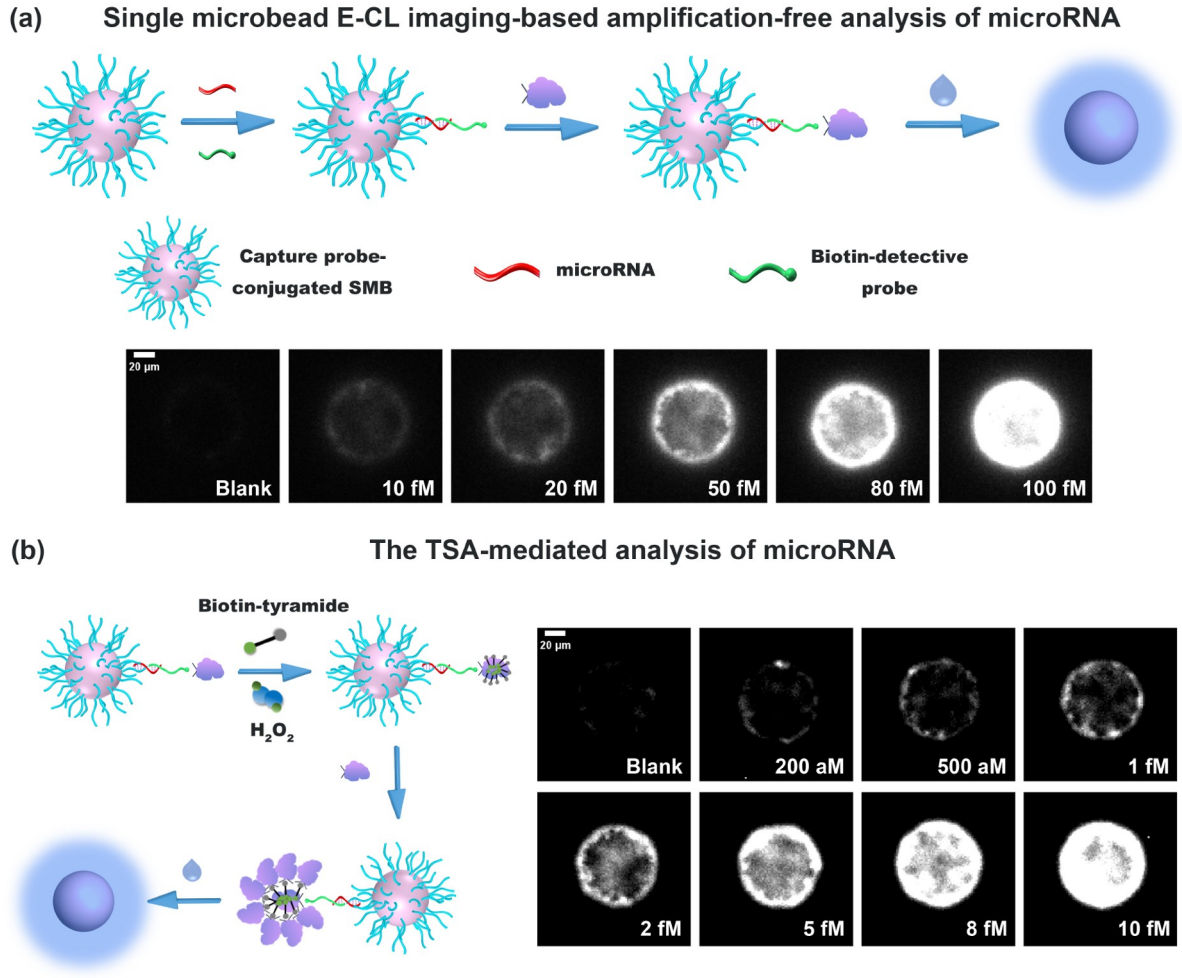

Figure 4 (Color online) (a) Schematic illustration (top panel) and the E-CL imaging results of the amplification-free let-7a microRNA assay based on the SMB CL imaging strategy via simple sandwich-type hybridization. (b) Schematic illustration (left panel) of the proposed SMB CL imaging strategy integrated with TSA-mediated amplification for microRNA detection, and the CL images of the single microbeads (right panel) for let-7a sensing based on TSA-mediated bioassay.

microRNA analysis can also be applied to the ultrasensitive analysis of a Hepatitis B Virus (HBV) DNA fragment (Figure S10). These results indicate that the SMB interfacial CL imaging strategy can be applied not only to immunoassay but also to detecting nucleic acid targets at the attomolar level, greatly broadening its application scope for the ultrasensitive detection of various critical biomarkers.

4 Conclusions

In summary, we have developed a new generation of single microbead E-CL imaging strategy, achieving significant advances in the ultrasensitive detection of protein, microRNA, and DNA biomarkers. With the aid of the powerful E-CL system and by "super-enriching" target-responsive HRP on the SMB, we have obtained an ultrastable, persistent, and high-intensity CL signal that is finely "super-confined" on the single microbead surface. This unique confinement not only capitalizes on the inherent advantages of CL imaging, such as the absence of external light excitation and high sensitivity but also enhances these benefits through the "super-enriching" effect. Furthermore, with the aid of TSA, our strategy has achieved an ultrahigh sensitivity, enabling the attomolar-level detection of proteins, microRNAs, and HBV DNA. In terms of practical clinical applications, it is anticipated that SMB-based assays can be further integrated with automated microfluidic systems. In this configuration, the SMB will be pre-arranged in a multichannel chip, thereby facilitating high-throughput detection and analysis. We believe that this single microbead E-CL imaging strategy possesses substantial potential for both fundamental research and clinical diagnostics.

Acknowledgements This work was supported by the National Natural Science Foundation of China (22074088, 22174091), the Program for Changjiang Scholars and Innovative Research Team in University (IRT_15R43), the Innovation Capability Support Program of Shaanxi (2025RS-CXTD-058), the Fundamental Research Funds for Central Universities (GK202301011) and the Shaanxi Province Postdoctoral Science Foundation (2023BSHEDZZ190).

Conflict of interest The authors declare no conflict of interest.

Supporting information The supporting information is available online at http://chem.scichina.com and http://link.springer.com/journal/11426. The supporting materials are published as submitted, without typesetting or editing. The responsibility for scientific accuracy and content remains entirely with the authors.

1 MacLean E, Broger T, Yerlikaya S, Fernandez-Carballo BL, Pai M, Denkinger CM. *Nat Microbiol*, 2019, 4: 748–758
2 Hu Q, Tong Z, Yalikong A, Ge LP, Shi Q, Du X, Wang P, Liu XY, Zhan W, Gao X, Sun D, Fu T, Ye D, Fan C, Liu J, Zhong YS, Jiang YZ, Gu H. *Nat Chem*, 2024, 16: 122–131
3 Jiang G, Liu H, Deng G, Liu H, Zhou Z, Ren T, Wang L, Zhang X, Yuan L. *Angew Chem Int Ed*, 2024, 63: e202400637
4 Shin H, Choi BH, Shim O, Kim J, Park Y, Cho SK, Kim HK, Choi Y. *Nat Commun*, 2023, 14: 1644
5 Shin H, Oh S, Kang D, Choi Y. *Adv Sci*, 2020, 7: 1903638
6 Ma F, Li Y, Tang B, Zhang C. *Acc Chem Res*, 2016, 49: 1722–1730
7 Chen W, Wang T, Dou Z, Xie X. *ACS Mater Lett*, 2020, 2: 1545–1554
8 Hayn M, John T, Bandak J, Rauch-Wirth L, Abel B, Münch J. *Adv Funct Mater*, 2024, 34: 2316260
9 Cai Q, Jin S, Zong H, Pei L, Cao K, Qu L, Li Z. *Anal Chem*, 2023, 95: 11641–11648
10 Li Y, Cu YTH, Luo D. *Nat Biotechnol*, 2005, 23: 885–889
11 Borgström E, Redin D, Lundin S, Berglund E, Andersson AF, Ahmadian A. *Nat Commun*, 2015, 6: 7173
12 Han M, Gao X, Su JZ, Nie S. *Nat Biotechnol*, 2001, 19: 631–635
13 Fan W, Dong Y, Ren W, Liu C. *TrAC Trends Anal Chem*, 2023, 162: 117035
14 Zheng B, Qin Y, Xiang Y, Guo A, Chen Y, Hu Y. *Anal Chem*, 2023, 95: 6542–6549
15 Chern M, Garden PM, Baer RC, Galagan JE, Dennis AM. *Angew Chem Int Ed*, 2020, 59: 21597–21602
16 Ruan Q, Macdonald PJ, Swift KM, Tetin SY. *Proc Natl Acad Sci USA*, 2021, 118: e2025033118
17 Xiao T, Zhao W, Han M, Huang X, Tang BZ, Chen Y. *Nano Today*, 2024, 59: 102522
18 Zhang Y, Li J, Zhu WH, Guo Z. *Sci China Chem*, 2025, 68: 26–34
19 Huang S, Bai S, Luo T, Feng B, Liu M, Zheng F, Huang S, Fang Y, Ding D, Zeng W. *Sci China Chem*, 2025, 68: 1175–1184
20 Chen Z, Li Q, Wu Y, Liu J, Liu L, Su L, Wu R, Song J. *Nat Commun*, 2025, 16: 238
21 Hananya N, Eldar Boock A, Bauer CR, Satchi-Fainaro R, Shabat D. *J Am Chem Soc*, 2016, 138: 13438–13446
22 Liu S, Li J, Zou Y, Jiang Y, Wu L, Deng Y. *Small*, 2023, 19: 2304631
23 Yang M, Huang J, Fan J, Du J, Pu K, Peng X. *Chem Soc Rev*, 2020, 49: 6800–6815
24 Chen X, Wang X, Fang Y, Zhang L, Zhao M, Liu Y. *Anal Chem*, 2022, 94: 8382–8391
25 Liu Y, Shen W, Li Q, Shu J, Gao L, Ma M, Wang W, Cui H. *Nat Commun*, 2017, 8: 1003
26 Zhang Z, Dong J, Yang Y, Zhou Y, Chen Y, Xu Y, Feng J. *Nat Commun*, 2023, 14: 7993
27 Wang Y, Wang M, Han L, Zhao Y, Fan A. *Talanta*, 2018, 182: 523–528
28 Li H, Liu C, Wang D, Zhang C. *Biosens Bioelectron*, 2017, 91: 268–275
29 Yu H, He Y. *Sens Actuat B-Chem*, 2015, 209: 877–882
30 Jiang T, Dai L, Lou Y, Wang H, Gao Z, Wu D, Ma H, Wei Q. *J Colloid Interface Sci*, 2025, 679: 780–787
31 Jiang T, Dai L, Lou Y, Wang H, Gao Z, Wu D, Ma H, Wei Q. *ACS Appl Mater Interfaces*, 2023, 15: 42404–42412
32 Zhou GH, Wang P, Yuan J, Qiu T, He ZK. *Sci China Chem*, 2011, 54: 1298–1303
33 Wang M, Shu J, Wang S, Lyu A, Wang Y, Huang D, Cui H. *Anal Chem*, 2023, 95: 12982–12991
34 Xu J, Wu J, Zong C, Ju H, Yan F. *Anal Chem*, 2013, 85: 3374–3379
35 Ouyang H, Xian J, Luo S, Zhang L, Wang W, Fu Z. *ACS Appl Mater Interfaces*, 2021, 13: 60945–60954
36 Wu H, Zhao M, Li J, Zhou X, Yang T, Zhao D, Liu P, Ju H, Cheng W, Ding S. *ACS Appl Mater Interfaces*, 2020, 12: 47270–47277
37 Lyu A, Wang Y, Cui H. *Anal Chem*, 2023, 95: 7914–7923
38 Deepa S, Venkatesan R, Jayalakshmi S, Priya M, Kim SC. *J Environ Chem Eng*, 2023, 11: 109853
39 Chen G, Jin M, Du P, Zhang C, Cui X, Zhang Y, Wang J, Jin F, She Y, Shao H, Wang S, Zheng L. *Food Agric Immunol*, 2017, 28: 315–327
40 Li N, Chen J, Luo M, Chen C, Ji X, He Z. *Biosens Bioelectron*, 2017, 87: 325–331
41 Li H, He Z. *Analyst*, 2009, 134: 800–804
42 Lyu A, Jin T, Wang S, Huang X, Zeng W, Yang R, Cui H. *Sens Actuat B-Chem*, 2021, 349: 130739

43 Xin L, Cao Z, Lau C, Kai M, Lu J. *Luminescence*, 2010, 25: 336–342
44 Tao X, Wang W, Wang Z, Cao X, Zhu J, Niu L, Wu X, Jiang H, Shen J. *Luminescence*, 2014, 29: 301–306
45 Marzocchi E, Grilli S, Della Ciana L, Prodi L, Mirasoli M, Roda A. *Anal Biochem*, 2008, 377: 189–194
46 Zhang X, Liu C, Wang H, Wang H, Li Z. *Angew Chem Int Ed*, 2015, 54: 15186–15190
47 Chen D, Zhang X, Zhu L, Liu C, Li Z. *Chem Sci*, 2022, 13: 3501–3506
48 Li L, Li J, Zhong M, Wu Z, Wan S, Li X, Zhang Y, Lv K. *Chem Eng J*, 2025, 503: 158093
49 Li N, Than A, Wang X, Xu S, Sun L, Duan H, Xu C, Chen P. *ACS Nano*, 2016, 10: 3622–3629
50 Maley AM, Garden PM, Walt DR. *ACS Sens*, 2020, 5: 3037–3042
51 Chen H, Li Z, Zhang L, Sawaya P, Shi J, Wang P. *Angew Chem Int Ed*, 2019, 58: 13922–13928
52 Rissin DM, Kan CW, Campbell TG, Howes SC, Fournier DR, Song L, Piech T, Patel PP, Chang L, Rivnak AJ, Ferrell EP, Randall JD, Provuncher GK, Walt DR, Duffy DC. *Nat Biotechnol*, 2010, 28: 595–599
53 Mao CP, Wang SC, Su YP, Tseng SH, He L, Wu AA, Roden RBS, Xiao J, Hung CF. *Sci Adv*, 2021, 7: eabg6522
54 Barya P, Xiong Y, Shepherd S, Gupta R, Akin LD, Tibbs J, Lee H, Singamaneni S, Cunningham BT. *Small*, 2023, 19: 2207239